Talanta 134 (2015) 627–639

Contents lists available at ScienceDirect

Talanta

journal homepage: www.elsevier.com/locate/talanta

Unveiling the identity of distant targets through advanced Raman-laser-induced breakdown spectroscopy data fusion strategies

Javier Moros, J. Javier Laserna *

Universidad de Málaga, Facultad de Ciencias, Departamento de Química Analítica, Campus de Teatinos s/n, 29071 Málaga, Spain

ARTICLE INFO

Article history:
Received 12 September 2014
Received in revised form
26 November 2014
Accepted 4 December 2014
Available online 13 December 2014

Keywords:
Spectroscopy
Data fusion
Laser-induced breakdown spectroscopy
Raman
Standoff

ABSTRACT

Data fusion is the process of combining data gathered from two or more sensors to produce a more specific, comprehensive and unified dataset of the inspected target. On this basis, much has been said about the possible benefits resulting from the use of molecular and atomic information for the detection of explosives. The orthogonal nature of the spectral and compositional information provided by Raman spectroscopy and laser-induced breakdown spectroscopy (LIBS) makes them suitable candidates for an optimal combination of their data, thus achieving inferences that are not feasible using a single sensor. The present manuscript evaluates several architectures for the combination of spectral outputs from these two sensors in order to compare the benefits and drawbacks of data fusion for improving the overall identification performance. From the simple assembling (concatenation or addition) of Raman and LIBS spectra to signals' processing on the basis of linear algebra (either the outer product or the outer sum), different identification patterns of several compounds (explosives, potential confusants and supports) have been built. The efficiency on target differentiation by using each of the architectures has been evaluated by comparing the identification yield obtained for all the inspected targets from correlation and similarity measurements. Additionally, a specific code integrated by several of these patterns to identify each compound has also been evaluated. This approach permits to obtain a better knowledge about the identity of an interrogated target, mainly in those decisive cases in which LIBS or Raman cannot be effective separately to reach a decision.

1. Introduction

Data fusion commonly refers to a process of combining synergistically or integrating, in the most effective way, observed data that gather from two or more sensors to produce a more specific, comprehensive and unified dataset of an interrogated target [1]. The benefits of data fusion have been used in a wide range of application fields. For instance, in the area of chemoinformatics, data fusion experiments have been made to combine several binary similarity coefficients to get an overall estimate of similarity for searching databases of bioactive molecules [2]. In environmental monitoring, spectral and structural datasets gathered from CASI (compact airborne spectrographic imager) and LIDAR (light detection and ranging) sensors, respectively, have been fused on a pixel level to improve the classification of the floodplain vegetation [3]. Similarly, ^{1}H NMR (nuclear magnetic resonance) information has been recently combined with mass spectrometry data from liquid [4] and gas [5] chromatography to generate metabolic profiles from analysis of rat urine as well as of cerebrospinal fluid of multiple sclerosis individuals, respectively. Information obtained by ^{1}H NMR has been also combined with UV–visible spectroscopy data [6] and with isotopic figures [7] to determine banned dyes in culinary spices and to improve the authenticity of wines, correspondingly.

New data fusion structures from chromatographic and spectroscopic data have been also proposed for improving the capability to identify the photoproducts formed and the accuracy in the description of the mechanism driving the photodegradation process [8]. The synergy of Raman and FT-NIR microscopies to enable a more complete visualization of any solid dosage pharmaceutical form has been demonstrated [9]. Likewise, in cultural heritage issues, data-fusion strategies based on the outputs of a Raman/X-ray fluorescence combined instrument, has been investigated for dealing with the classification of ochre pigments [10]. Furthermore, complementary spectra from Raman, IR (infrared) and NMR sources have been assembled for giving a "*fused*" dataset to an increased understanding and control of an industrial process [11]. Also for solving problems related to food authentication, data collected from near (NIR) and middle (MIR) infrared spectrometers have been processed both, separately and jointly, using chemometrics to demonstrate the synergistic effect from fused spectroscopic datasets for dealing with classification problems [12,13]. In the same vein, data from mass spectra (MS)-based electronic nose (E-nose), a mid-IR optical-tongue

* Corresponding author. Tel.: +34 952 13 1881; fax: +34 952 13 2000.
E-mail address: laserna@uma.es (J. Javier Laserna).

http://dx.doi.org/10.1016/j.talanta.2014.12.001
0039-9140/

and a UV–visible sensor have been assembled to deal with differences from sensory properties on beer samples of the same brand and commercialized as a same product, but brewed in four different factories [14]. Equally, a data fusion strategy of combining multiple spectroscopic techniques (NIR, Raman, 2D fluorescence and X-ray fluorescence) has been also investigated for the characterization of soy hydrolysates in mammalian cell cultures [15]. In the area of homeland security, an approach for the combination of the spectral outputs of sensors based on Raman and LIBS (Laser-Induced Breakdown Spectroscopy) in order to improve the identification of explosives and related compounds has been developed [16]. However, despite the improvement on materials distinction from each other by simple linear correlation when molecular information is merged to atomic data, the progress of selectivity towards specificity is still being pursued.

Detection of explosives has attracted considerable attention in recent years [17]. From the standpoint of sensor fusion, the most appealing tools to tackling this scenario have proved to be LIBS [18] and Raman spectroscopy [19]. Together with their versatility to operate under a standoff scheme, both sensing modes offer complete information on the constitution of the sample, that is, elemental composition from the emission spectra and molecular information extracted from scattered radiation. Commonly, to deal with such challenge both techniques are used separately. At these circumstances, that is, when findings are judged on the basis of particular spectral information, the decision about target's identity might be limited. For instance, LIBS has a restricted ability on identify those inspected targets that share elemental composition, as organics [20]. Similarly, although interaction between excitation light and the target might lead to a unique spectral fingerprinting of the material, selectivity of Raman suffers when the same functional group is involved in the composition of the interrogated targets [21]. Clearly, these particular scenarios entail a deficit for each spectroscopic technique, notably when trying to differentiate between explosive and harmless materials.

Assembling and integration of such techniques into a mobile sensor platform using the same laser pulses and gated multichannel detectors to improve identification confidence has been demonstrated [22]. Despite that this fitting of the two sensors allows to simultaneously gather both spectral data coming from the same laser events, the manner in how such information may be manipulated and also associated has still a lot of grounds for concern. The reason is due to some technical incompatibilities, especially when it comes to residue analysis [23]. Indeed, to date, only a few attempts on fusion of these data, although acquired from a sequential interrogation of bulk targets, have been recently published [16,24].

In order to progress, in the present manuscript, several novel architectures on assembling data from Raman and LIBS sensors are described. The strengths and the weaknesses of several estimators built to provide a precise identification of pure materials have been evaluated through correlation and dissimilarity measurements. Results on the implementation of such assets in order to enhance the differentiation and recognition of inspected targets have been discussed. Findings have revealed that the combination of different bidimensional assembling frameworks fused into a unique estimator may provide a reliable attribute to confidently label the identity of each interrogated target.

2. Experimental

2.1. Sensor set-up

The versatile Raman and LIBS configurable set-up for standoff analysis consisted of twins Q-switched Nd:YAG lasers (10 Hz, 532 nm, 400 mJ pulse^{-1}, 5.5 ns pulse width) that were utilized as irradiative sources. A beam expander (10 × large output) was employed for first expanding and then focusing the laser beam on the target. Scattered and emitted light from the target was gathered through a home-made Cassegrain telescope (167 cm in length and 24 cm in diameter), which permits converging light on the tip of an optical fiber 600 μm in diameter mounted on a precision linear stage. After collection, light was guided to the entrance port of the proper detection system.

For Raman data collection, a holographic imaging spectrograph (85 mm focal length, *f*/1.8*i*, 25 μm slit) equipped with a volume phase holographic (VPH) grating (model HSG-532-LF) and fitted with an iCCD detector (intensifier tube diameter of 18 mm) was used. For LIBS signal detection, a Czerny–Turner spectrograph (303 mm focal length, *f*/4, 10 μm slit) fitted with a 150 lines per mm diffraction grating blazed at 500 nm and an iCCD detector (intensifier tube diameter of 25 mm) was employed.

Raman and LIBS measurements were sequentially obtained for each target after focusing a number of laser pulses of 440 mJ each on sections of ca. 1.00 cm^2 and 0.02 cm^2, thus achieving irradiance values of 0.11 GW cm^{-2} and 4.73 GW cm^{-2}, respectively. For Raman data collection, the delay time was set to zero ns, whereas the gate width was set to 800 ns. For LIBS data acquisition, a delay time of 900 ns and an integration time of 9 μs were established as timing parameters. Experiments were all carried out at standoff distances of 20 m inside a 50 m long partially closed corridor. Data obtained from Andor were exported in text format and analyzed using Matlab® (The Mathworks Inc., South Natick, MA, USA). In any case, readers requiring more details are requested to check the reference [23].

2.2. Samples

In order to evaluate the strength and weaknesses on the implementation on data fusion from different strategies, Raman and LIBS representative spectra from pure explosive materials, including 2,6-dinitrotoluene (DNT), 2,4,6-trinitrotoluene (TNT), cyclotrimethylenetrinitramine (RDX), pentaerythritoltetranitrate (PETN) as well as some explosive related compounds (ERCs) such as sodium chlorate ($NaClO_3$) and potassium chlorate ($KClO_3$), were registered. In parallel, several non-energetic materials, but subject to confusion with the previous ones from their LIBS responses, such as nylon, wood, riblene (low density polyethylene), anthracene (anth), sodium chloride (NaCl) and potassium chloride (KCl) were also considered.

Samples were primed and arranged for the analysis in their most appropriate bulk form. Thus, DNT, $NaClO_3$, $KClO_3$, anth, NaCl and KCl were used as cylindrical pellets of ca. 200 mm^2 in area and 6 mm in thickness. In addition, RDX base paste explosive was prepared as a sticky mass on the surface of a glass microscope slide (76 mm × 26 mm), at all times, helping to safeguard dimensions (thickness and area) similar to those achieved for the previously cited pellets. Similar case held true for TNT, from its melted solid form. Finally, PETN, extracted as a ring from a booster, as well as Nylon, wood and Riblene, all them as plates (40 mm × 40 mm × 4 mm), were analyzed in their raw state. In this way, all the targets were tested as bulk materials.

2.3. Raman-LIBS data fusion approaches

The fusion process at the feature level of spectral responses from sensor measurements consists in the generation of a new attribute, that is, a new identity which aims to more clearly identify the interrogated target. To this end, a global descriptor of the compound is generated by fusing the molecular and atomic outputs of a compound when interrogated by Raman and LIBS sensors.

In this particular case, although spectral information gathered by our dual sensor, comes from different regions of the sample and the Raman and LIBS responses arise from different laser events, complete spectroscopic information faithfully represents the target under interrogation. To construct the new attributes of each compound, representative Raman and LIBS spectra were used.

For this purpose, first, scattered light resulting from 25 sequential laser pulses on the target surface was accumulated for building up the final Raman response. There was no evidence that the use of these successive laser pulses produced any photo and/or thermal surface degradation. Meanwhile, the emitted light from additional 25 laser-induced plasmas was averaged to yield the LIBS counterpart.

Due to the different dynamic ranges of the Raman and LIBS responses, normalization by scaling between 0 and 1 was considered. It was further verified that performance of the parameters indicating the degree of similarity is preserved, no matter how the normalization approach proceeds. However, such type of scaling not only ensures the distinction between new identifiers on the basis of the different frequencies and wavelengths of the spectral features but also provides an equally input of the molecular and atomic information for the final attribute, whatever the assembling mode used. Without this last, comparison of the new identifiers would be equivalent to compare information from a single sensor, that is, the dataset involving a largest weight in the attribute. A more detailed description on the min-max scaling method may be found in a previous Ref. [16].

For convenience of the reader, the present section has been divided according the vector or matrix nature of the new attribute generated. As starting information for the 4 approaches developed it has taken the intensity values belonging to the Raman (r) and LIBS (l) spectra at each relevant pixel ($n=1, 2, 3,\ldots,1665$) and arranged into two separate identical-size vectors, named R (Raman) and L (LIBS), respectively.

- New attributes as a first-order vectors
  - Vectors concatenation

    There are a number of different techniques for synthesizing a fused attribute. The technique used as first instance, concatenative synthesis, relies on concatenation of the Raman and LIBS spectra from each compound to construct its new identifier. The final attribute is constructed from an augmented vector built by correlatively allocating the LIBS data (spanning the spectral range from 320 nm up to 780 nm) together with the Raman counterpart (containing frequencies between 400 cm^{-1} and 1800 cm^{-1}). Thus, the new identifier consists of a vector of 3330 variables.

$$\begin{bmatrix} r_1 & r_2 & r_3 & r_4 & r_5 & \ldots & r_n \end{bmatrix} \begin{bmatrix} l_1 & l_2 & l_3 & l_4 & l_5 & \ldots & l_n \end{bmatrix} = \begin{bmatrix} r_1 & r_2 & r_3 & r_4 & r_5 & \ldots & r_n & l_1 & l_2 & l_3 & l_4 & l_5 & \ldots & l_n \end{bmatrix}$$

  - Vectors coaddition

    Another straightforward process, like the concatenative synthesis, is the coaddition technique. This time, taking advantage on the availability of a same number of variables for both spectra, the sum, pixel to pixel, of Raman and LIBS responses is considered for generating a composite attribute to each compound. Through this procedure, the new attribute preserves their vector form and the number of variables (1665), but changes its shape according to the Raman and LIBS information. Despite that this new attribute is also built from the complete molecular and atomic spectral information, it should be pointed out that it has no longer meaning in terms of spectroscopy.

$$\begin{bmatrix} r_1 & r_2 & r_3 & r_4 & r_5 & \ldots & r_n \end{bmatrix} + \begin{bmatrix} l_1 & l_2 & l_3 & l_4 & l_5 & \ldots & l_n \end{bmatrix} = \begin{bmatrix} r_1+l_1 & r_2+l_2 & r_3+l_3 & r_4+l_4 & r_5+l_5 \ldots r_n+l_n \end{bmatrix}$$

- New attributes as a second-order vectors
  - Vectors outer sum

    The tensorial sum of two vectors is a way of creating a new space on the basis of sum of integers. As shown below, data produce a fused square array (1665×1665) when associated by summing each pixel of the transposed L vector to every pixel of the R vector.

$$\begin{bmatrix} r_1 \\ r_2 \\ r_3 \\ r_4 \\ r_5 \\ \ldots \\ r_n \end{bmatrix} \oplus \begin{bmatrix} l_1 & l_2 & l_3 & l_4 & l_5 & \ldots & l_n \end{bmatrix} = \begin{bmatrix} r_1+l_1 & r_2+l_1 & r_3+l_1 & r_4+l_1 & r_5+l_1 & \ldots & r_n+l_1 \\ r_1+l_2 & r_2+l_2 & r_3+l_2 & r_4+l_2 & r_5+l_2 & \ldots & r_n+l_2 \\ r_1+l_3 & r_2+l_3 & r_3+l_3 & r_4+l_3 & r_5+l_3 & \ldots & r_n+l_3 \\ r_1+l_4 & r_2+l_4 & r_3+l_4 & r_4+l_4 & r_5+l_4 & \ldots & r_n+l_4 \\ r_1+l_5 & r_2+l_5 & r_3+l_5 & r_4+l_5 & r_5+l_5 & \ldots & r_n+l_5 \\ \ldots & \ldots & \ldots & \ldots & \ldots & \ldots & \ldots \\ r_1+l_n & r_2+l_n & r_3+l_n & r_4+l_n & r_5+l_n & \ldots & r_n+l_n \end{bmatrix}$$

  - Vectors outer product

    Similarly to the previous approach, the tensorial product (also named outer product) of two vectors allows to create a new space equivalent to multiplication of integers. On this occasion, the new attribute is, again, a 1665-by-1665 block matrix formed from all possible products between the elements of R and those of L.

$$\begin{bmatrix} r_1 \\ r_2 \\ r_3 \\ r_4 \\ r_5 \\ \ldots \\ r_n \end{bmatrix} \otimes \begin{bmatrix} l_1 & l_2 & l_3 & l_4 & l_5 & \ldots & l_n \end{bmatrix} = \begin{bmatrix} r_1l_1 & r_2l_1 & r_3l_1 & r_4l_1 & r_5l_1 & \ldots & r_nl_1 \\ r_1l_2 & r_2l_2 & r_3l_2 & r_4l_2 & r_5l_2 & \ldots & r_nl_2 \\ r_1l_3 & r_2l_3 & r_3l_3 & r_4l_3 & r_5l_3 & \ldots & r_nl_3 \\ r_1l_4 & r_2l_4 & r_3l_4 & r_4l_4 & r_5l_4 & \ldots & r_nl_4 \\ r_1l_5 & r_2l_5 & r_3l_5 & r_4l_5 & r_5l_5 & \ldots & r_nl_5 \\ \ldots & \ldots & \ldots & \ldots & \ldots & \ldots & \ldots \\ r_1l_n & r_2l_n & r_3l_n & r_4l_n & r_5l_n & \ldots & r_nl_n \end{bmatrix}$$

By plotting any of new attributes before mentioned, a final distinct pattern, for a precise identification of each compound, is reached. Again, these new discrete projections have no meaning in terms of spectroscopy. On the whole, these different attributes just

Table 1
Values for the correlation coefficient (r) and the root mean square error (*RMSE*) estimated between assayed compounds from their normalized LIBS (top) and Raman (bottom) responses[a].

		Organic compounds								Inorganic compounds			
		DNT	TNT	RDX	PETN	nylon	wood	riblene	anth	NaCl	$NaClO_3$	KCl	$KClO_3$
Organic compounds	DNT		0.1165	0.1222	0.1770	0.0536	0.1340	0.0875	0.1313	0.2105	0.1979	0.1808	0.1889
	TNT	0.7902		0.1076	0.1580	0.1597	0.2092	0.1854	0.2292	0.2042	0.1768	0.2091	0.2179
	RDX	0.6174	0.7552		0.1171	0.1437	0.1581	0.1508	0.1843	0.1979	0.1815	0.1576	0.1671
	PETN	0.2199	0.2637	0.5156		0.1852	0.1663	0.1840	0.2115	0.1981	0.1860	0.1827	0.1898
	nylon	0.9612	0.6279	0.5417	0.2534		0.1078	0.0461	0.0948	0.2168	0.2095	0.1738	0.1813
	wood	0.7955	0.5233	0.5905	0.5573	0.8568		0.0926	0.1049	0.2250	0.2232	0.1740	0.1698
	riblene	0.9034	0.5053	0.5033	0.2842	0.9741	0.8724		0.0665	0.2127	0.2099	0.1570	0.1639
	anth	0.8718	0.4540	0.4409	0.2609	0.9408	0.8364	0.9661		0.2227	0.2296	0.1640	0.1695
Inorganic compounds	NaCl	0.1336	-0.0058	0.0053	0.1117	0.1771	0.2580	0.2339	0.3396		0.0443	0.1999	0.2011
	$NaClO_3$	0.1189	0.0024	0.0113	0.0852	0.1582	0.2646	0.2107	0.3031	0.9855		0.1987	0.2000
	KCl	0.3360	0.1190	0.2386	0.1041	0.4065	0.3857	0.4732	0.4755	0.2362	0.2196		0.0342
	$KClO_3$	0.3231	0.1270	0.2316	0.1205	0.3887	0.4435	0.4545	0.4538	0.2876	0.2903	0.9683	

		Organic compounds								Inorganic compounds			
		DNT	TNT	RDX	PETN	nylon	wood	riblene	anth	NaCl	$NaClO_3$	KCl	$KClO_3$
Organic compounds	DNT		0.1044	0.1464	0.1573	0.3112	0.1420	0.2473	0.1342	0.1420	0.1533	0.1420	0.1539
	TNT	0.8144		0.1733	0.1478	0.2391	0.2057	0.1967	0.1772	0.2057	0.2069	0.2057	0.2066
	RDX	0.0220	-0.0116		0.1355	0.3180	0.1357	0.2437	0.1278	0.1357	0.1411	0.1357	0.1414
	PETN	-0.0440	0.0406	0.2031		0.2610	0.1754	0.1930	0.1493	0.1754	0.1748	0.1754	0.1745
	nylon	0.2674	0.4230	0.1116	0.2908		0.3880	0.1539	0.3430	0.3880	0.3790	0.3880	0.3784
	wood	NaN	NaN	NaN	NaN	NaN		0.3100	0.0935	0.0000	0.0706	0.0000	0.0732
	riblene	0.1119	0.0978	0.1290	0.2258	0.5586	NaN		0.2658	0.3100	0.3032	0.3100	0.3018
	anth	0.0126	-0.0127	0.0128	-0.0066	0.0192	NaN	0.0483		0.0935	0.1092	0.0935	0.1097
Inorganic compounds	NaCl	NaN	NaN	NaN	NaN	NaN	NaN	NaN	NaN		0.0706	0.0000	0.0732
	$NaClO_3$	-0.0957	-0.0766	0.0318	0.0188	0.0050	NaN	-0.0247	-0.0154	NaN		0.0706	0.0347
	KCl	NaN	NaN	NaN	NaN	NaN	NaN	NaN	NaN	NaN	NaN		0.0732
	$KClO_3$	-0.1052	-0.0842	0.0258	0.0095	-0.0210	NaN	-0.0188	-0.0126	NaN	0.8770	NaN	

[a] Light-gray cells contain *RMSE* values whereas non colored cells list r values. *NaN* (no available number) reflects the impossibility for computing the parameter when the signal is a vector completely composed by zeros.

represent distinct guides which can be used, separately or together, to identify an unknown target.

2.4. Data analysis

The goal of any data fusion approach aimed to enhance the identity of a target is the building of a new attribute, from its sensor responses, that completely differs from the attribute generated for any other target. Assessment of the new attribute quality was carried out by using the correlation coefficient value (denoted by r). Thus, supposing that A and B are two finite-size attributes (either vectors or matrices), r is computed from Eq. (1) as follows:

$$r = \frac{\Sigma_m \Sigma_n (A_{mn} - \overline{A})(B_{mn} - \overline{B})}{\sqrt{\left(\Sigma_m \Sigma_n (A_{mn} - \overline{A})^2\right)\left(\Sigma_m \Sigma_n (B_{mn} - \overline{B})^2\right)}} \quad (1)$$

where $\overline{A}$ and $\overline{B}$ are the mean values of the elements composing A and B, respectively. As a result, the closer is the value of r to 1, the higher the similarity between the attributes under consideration and, consequently, more problematic is their identification. However, as r depends only on the shapes of new attributes, not on their magnitudes, an additional measure of the extent to which a pair of attributes is similarly related was also computed through the root mean square error (*RMSE*), which has been a dominant quantitative performance metric in the field of signal processing. The aim of this measure is to compare two attributes by providing a quantitative score that describes the degree of similarity or, conversely, the level of error between them. *RMSE* between two attributes is calculated from Eq. (2):

$$RMSE = \sqrt{\frac{1}{NM}\sum_{n,m}\{A(n,m) - B(m,n)\}^2} \quad (2)$$

where NM is the total number of variables in each attribute. In this case, the lower the *RMSE* value the greater the similarity between the attributes from compounds being compared. Consequently, the system bears a substantial difficulty in distinguishing them.

These parameters are highly useful for assessing the level of identity for an unknown target via the matching of its attribute and concrete attributes for compounds of interest constructed in advance and included in a short library.

3. Results and discussion

3.1. Differentiating compounds from single technique responses

As discussed elsewhere [23], both Raman and LIBS sometimes may fail on providing a genuine spectral fingerprint to unequivocally identify a compound. In order to tinge this pronouncement, both the LIBS and Raman spectra of a number of explosives and related compounds have been compared using their correlation coefficients and root mean square errors. Table 1 summarizes the corresponding values. As seen, for different pairs of compounds, the exclusive use of information from the LIBS sensor prevents a reliable categorization of a compound as an explosive or a harmless material. According to the standoff spectral response uncertainty, a correlation coefficient of 0.8 was considered a limiting value for discrimination purposes. Decisions on disparity

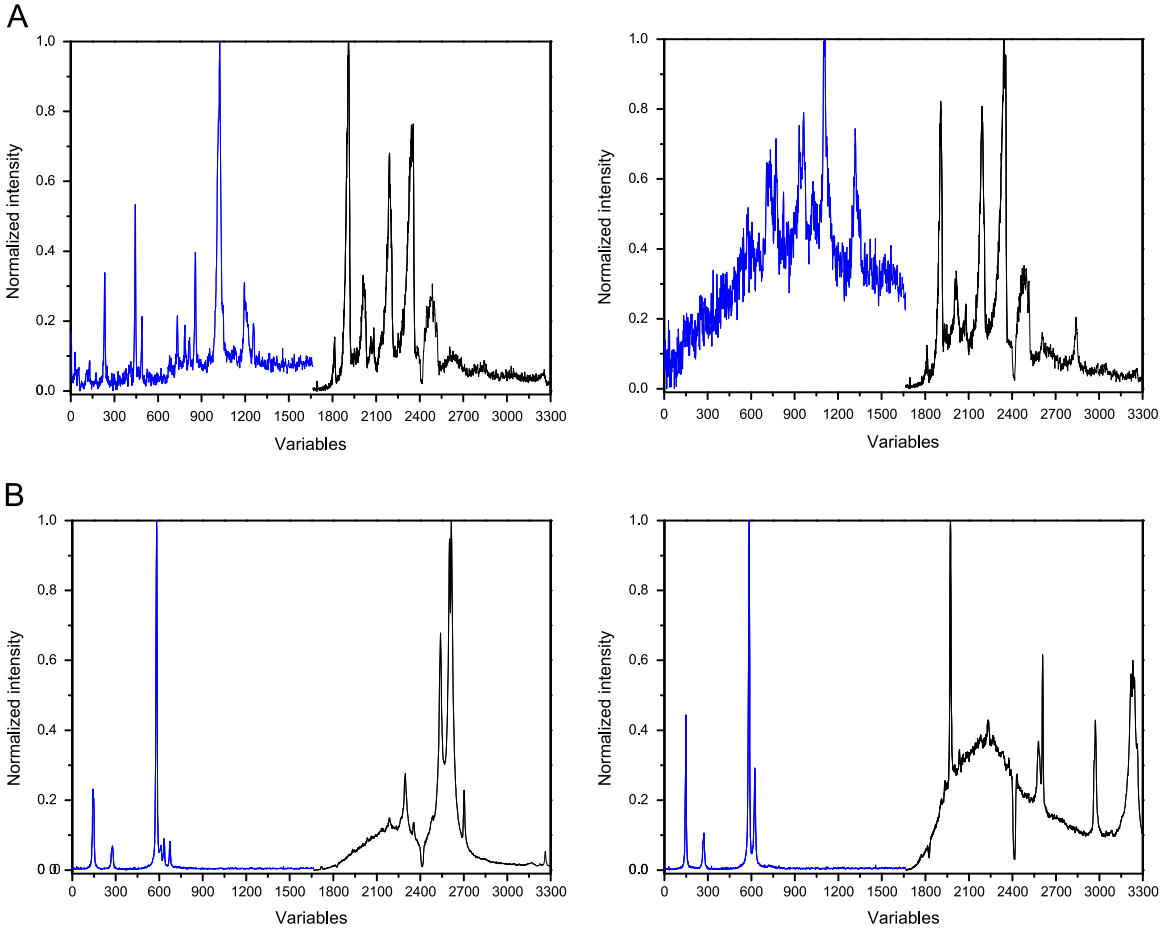

Fig. 1. Paired comparison of the resulting attributes from the concatenation of the Raman and LIBS normalized information for (A) DNT and nylon and (B) $NaClO_3$ and $KClO_3$.

between compounds whose *r* values are larger than this threshold might be imprecise. For instance, differentiation between DNT and nylon (0.9612), riblene (0.9034) and anth (0.8718), is unconfident on the sole basis of their LIBS spectra. In a similar fashion, *RMSE* values keep consistently low for the pairs considered; −0.0536, 0.0875, and 0.1313, respectively. Similarly, decisions based on Raman spectra may also be compromised as seen for DNT and TNT or the chlorates examined with respective *r* values of 0.8144 and 0.8770. To cope with these difficulties, an investigation on new approaches for creating new identification patterns by fusing Raman and LIBS information has been tackled.

3.2. Differentiating compounds using first-order attributes

The easiest way to proceed in data fusion is the concatenation of the spectral information, that is, a correlative allocation of the LIBS outcome together with its Raman counterpart. Fig. 1 depicts an example of the new estimators generated by concatenation for two pairs of interest. The left side represents the Raman contribution to the estimator, whereas the right part accounts for the LIBS involvement. As shown, for the couple DNT–nylon, the LIBS input retains the envisaged similarity between the compounds, whereas the Raman participation acts as the crucial component that may contribute to a successful differentiation between them. In other instances it is the LIBS data set the key factor to discern the compounds as is the case of the pair $NaClO_3$–$KClO_3$.

By stacking the paired outcomes at variable level, coaddition of data produces a simple and common output, which acts later as the input for the final decision. Fig. 2 displays the attributes for the case of DNT and NaCl. Differently from the concatenation framework, coadding the data leads to a new identity lacking of direct spectral interpretation. As seen, the molecular and the atomic information intermingle with each other within a new and intricate attribute built for DNT. In contrast, a compound of missing Raman response produces an attribute identical to the LIBS spectrum. This is the case of NaCl shown in the figure.

The effectiveness of all these new attributes for differentiation between compounds is evaluated from the results listed in Table 2. The correlation coefficients together with *RMSE* values for the new estimators are summarized. As reflected, both approaches successfully solve conflicting situations related to organic compounds. For instance, when the performance of the new estimators is compared with the sole use of LIBS information, the *r* values for the pairs DNT–nylon, DNT–riblene and DNT–anth, stand close to 0.6. Simultaneously, their *RMSE* values scale beyond 0.1 on a proportional basis in accordance with the decreasing values of *r*. Raman information produces significant synergistic effects for differentiation.

However, conflicts concerning the differentiation between chloride and chlorate from the same cation remain with *r* values close to 0.9 and *RMSE* results below 0.1. In this particular case, the new attributes offer only a modest improvement as compared to the simple LIBS information. In other words, the merging of Raman information brings no significant advance in the distinction between such compounds. Hence, this implies the need of alternative approaches for assembling the spectral information to cope with such unfavorable cases.

3.3. Differentiating compounds using second-order attributes

Once evaluated the performance of first-order attributes, fusion approaches were focused on the generation of second-order characteristic estimators for each compound. By building 2D images from these final patterns, new identities for each compound are achieved. Fig. 3 depicts the 2D images generated for DNT and NaCl, respectively, from the outer sum (top) and the outer product (bottom) of their particular Raman and LIBS responses. Since these operations are

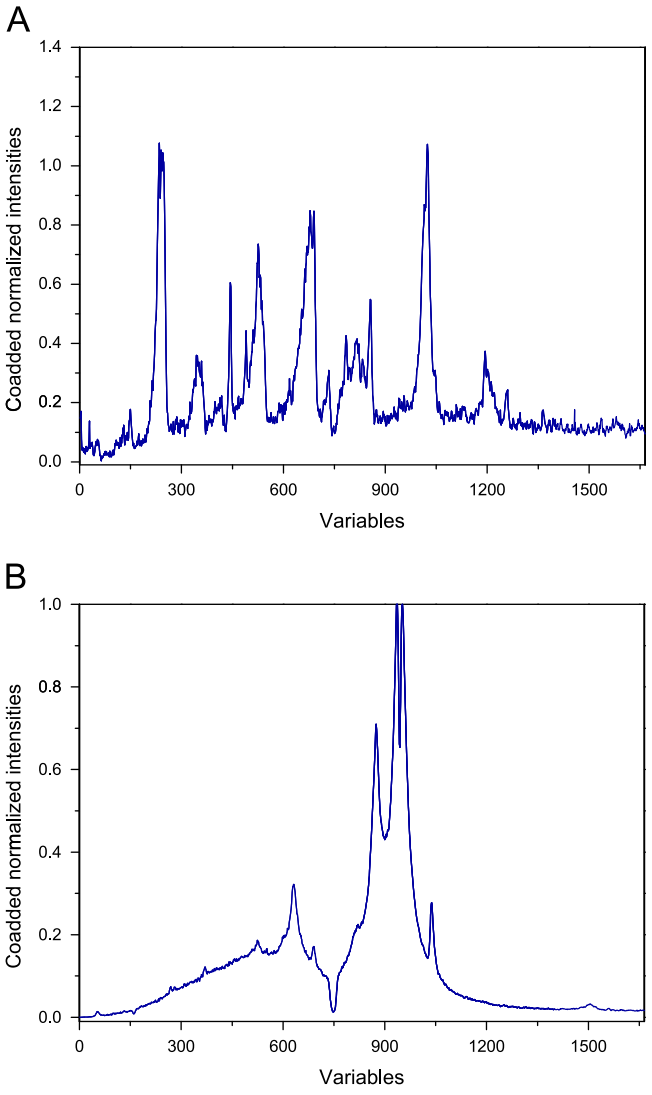

Fig. 2. Examples of the resulting attributes from the coaddition of the Raman and LIBS normalized information for (A) DNT and (B) NaCl.

performed on vectors of identical size, the final outcome leads to a square matrix of ca. 2.8 million variables in both instances. As shown, in the case of the outer sum, fusion of paired spectral variables yields a complex additive contribution to each point of the image, thereby highlighting the complete molecular and atomic information. In contrast, when fusion is based on the product of variables, any lack of spectral features within one of the counterparts cancels the information of the other. That is the reason why, in the case of DNT, only the concurring atomic and molecular signals account for the emphasized features within the final 2D image. On the contrary, for NaCl, the absence of Raman response leads to a final image consisting solely of zeros, the attribute in this case still being fully descriptive.

The significance of these 2D images on compound differentiation may be assessed from the results reported in Table 3. The similarity between the corresponding 2D images was evaluated by means of values of *r* and *RMSE*. As observed, the sum-based identifiers perform similarly to the corresponding first order attributes (see Table 2). For instance, correspondence between DNT and nylon, riblene and anth, fits to *r* values of 0.6727 (0.5088 and 0.6404), 0.6342 (0.5472 and 0.6119) and 0.6628 (0.6265 and 0.6795), respectively. This evidence is also supported by parallel *RMSE* values. Something similar holds true for the *chloride–chlorate* pairs for

Table 2
Values for the correlation coefficient (r) and the root mean square error (*RMSE*) estimated between assayed compounds from first-order attributes generated by concatenation (top) and coaddition (bottom) of their Raman and LIBS responses[a].

		Organic materials								Inorganic materials			
		DNT	TNT	RDX	PETN	nylon	wood	riblene	anth	NaCl	$NaClO_3$	KCl	$KClO_3$
Organic materials	DNT		0.1106	0.1349	0.1674	0.2233	0.1380	0.1855	0.1328	0.1796	0.1770	0.1626	0.1723
	TNT	0.6306		0.1442	0.1530	0.2033	0.2075	0.1911	0.2049	0.2050	0.1925	0.2074	0.2123
	RDX	0.3893	0.2072		0.1266	0.2468	0.1473	0.2026	0.1586	0.1697	0.1626	0.1471	0.1548
	PETN	0.1195	0.1744	0.3592		0.2263	0.1709	0.1885	0.1831	0.1871	0.1804	0.1791	0.1823
	nylon	0.5088	0.6345	0.1700	0.2669		0.2847	0.1136	0.2517	0.3143	0.3062	0.3006	0.2967
	wood	0.5773	-0.0502	0.4610	0.3041	0.0882		0.2287	0.0994	0.1591	0.1655	0.1230	0.1307
	riblene	0.5472	0.4240	0.2421	0.2734	0.8211	0.2948		0.1937	0.2658	0.2608	0.2457	0.2428
	anth	0.6265	-0.0261	0.3604	0.1279	0.2028	0.8374	0.4126		0.1708	0.1798	0.1335	0.1428
Inorganic materials	NaCl	0.1478	-0.2152	0.0990	0.0444	-0.1433	0.4618	-0.0077	0.4708		0.0589	0.1414	0.1513
	$NaClO_3$	0.0964	-0.1732	0.0847	0.0371	-0.0896	0.3799	0.0106	0.3694	0.8955		0.1491	0.1435
	KCl	0.2620	-0.3114	0.2703	-0.0054	-0.2412	0.6671	-0.0455	0.6289	0.4836	0.3716		0.0571
	$KClO_3$	0.2264	-0.2821	0.2548	0.0138	-0.1985	0.6409	-0.0188	0.5720	0.4721	0.5080	0.9204	

		Organic materials								Inorganic materials			
		DNT	TNT	RDX	PETN	nylon	wood	riblene	anth	NaCl	$NaClO_3$	KCl	$KClO_3$
Organic materials	DNT		0.1243	0.1685	0.2142	0.3396	0.1440	0.3004	0.1655	0.2441	0.2496	0.1974	0.2229
	TNT	0.7344		0.1645	0.1897	0.3524	0.1889	0.3234	0.2168	0.2334	0.2367	0.1838	0.2105
	RDX	0.5024	0.3460		0.1856	0.3504	0.1580	0.3012	0.1896	0.2151	0.2155	0.1774	0.1955
	PETN	0.3455	0.3323	0.4038		0.3179	0.1693	0.2790	0.2063	0.2578	0.2585	0.2078	0.2112
	nylon	0.6404	0.3772	0.4137	0.4066		0.3429	0.1428	0.2681	0.4406	0.4518	0.3679	0.3603
	wood	0.6859	0.3266	0.5669	0.6436	0.7075		0.2908	0.1466	0.2250	0.2224	0.1740	0.1868
	riblene	0.6119	0.2086	0.4639	0.3941	0.8200	0.7747		0.2239	0.4028	0.4099	0.3239	0.3157
	anth	0.6795	0.2480	0.4746	0.3913	0.7726	0.7873	0.7909		0.2656	0.2725	0.1990	0.2106
Inorganic materials	NaCl	0.1613	0.0695	0.3053	0.2864	0.4112	0.2580	0.3333	0.3150		0.0769	0.1999	0.2257
	$NaClO_3$	0.1079	0.0245	0.3059	0.3024	0.3601	0.2737	0.3208	0.2780	0.8903		0.1967	0.2038
	KCl	0.2064	0.0114	0.1772	0.1794	0.3819	0.3857	0.3611	0.4085	0.2362	0.2564		0.0823
	$KClO_3$	0.1526	-0.0096	0.1986	0.2444	0.3263	0.4092	0.3392	0.3562	0.2536	0.4443	0.8737	

[a] Light-gray cells contain *RMSE* values whereas non colored cells list the r values.

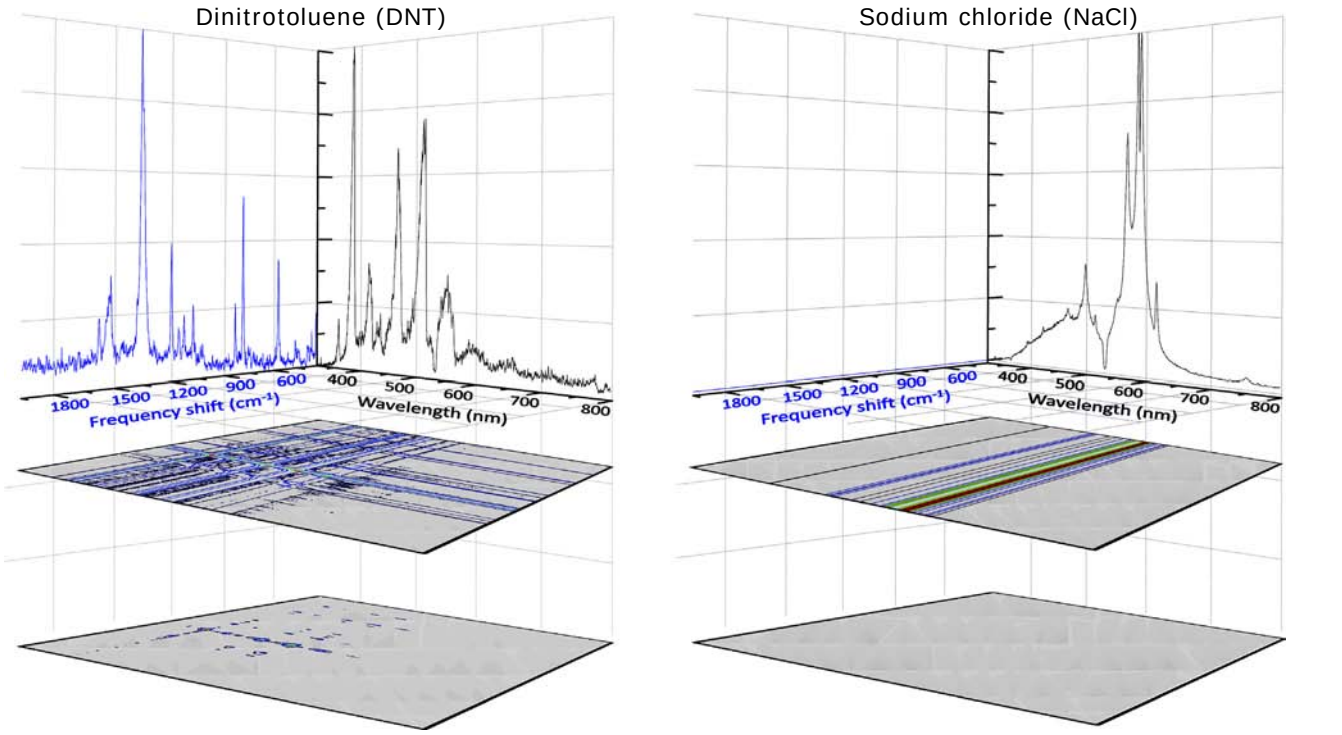

Fig. 3. Examples of the second order estimators resulting either from the outer sum (top) and the outer product (bottom) of the particular Raman and LIBS responses for DNT (on the left) and NaCl (on the right).

which such assembling still fails to satisfactorily solve their sorting, as revealed by r values larger than 0.8.

A different instance occurs with the product-based images. While these new identities seem limited in their identificative abilities, their manifested specificities are much larger than those of sum 2D images. Proof of this can be found in the markedly shrink of the r values for the pairs DNT–riblene and DNT–anth, 0.4703 and 0.2271, respectively. Likewise, in the cases of the pairs $NaClO_3$–NaCl and $KClO_3$–KCl, the lack of Raman response for chlorides results in a positive synergy in the final 2D estimator for their subsequent differentiation from their respective chlorates. Due to the infinitesimal impact of quadratic residuals, dissimilarity rates (*RMSE*) between these product-based 2D images are one order of magnitude lower than those of the other attributes. Though this circumstance could suggest a larger similarity between the identities being compared, the correlation values demonstrate that such a fusion process generates new attributes, which lead to a correct distinction between those compounds. A significant limitation of the product-based approach arises for compounds lacking of a Raman response. Under these circumstances, the final outcome of the assembling procedure is a zero (null) matrix, thereby voiding any benefit provided by their LIBS information; for instance, NaCl is identical to KCl, in spite of the large difference in their atomic composition. Notwithstanding this, second order data assembling is more favorable to solve the most conflicting cases, that is, between explosives and confusants.

3.4. Peer-to-peer assessment of image quality

Having assessed the differentiation capabilities of these new 2D images, their quality for identification purposes was contrasted with 2D attributes built beforehand [16]. To that end, the universal image index of quality (IOQ) proposed by Wang and Bovik was used [25]. With a value range of $[-1, 1]$, such index denotes the matching between two images, the closer the value to 1 the more similar are the images. The resulting outcomes from this peer comparison are summarized in Table 4.

Consider the distinction between hazardous (DNT, TNT, RDX and PETN) and harmless (nylon, wood, riblene and anth) organics. When using 2D images based on the outer sum, no identity differences between the explosives and anthracene are noticed (IOQ outcome above the limiting value of 0.8 needed for discrimination). Similar holds true for other pairs like DNT–wood and PETN–riblene. In contrast, hazardous organics are discernible when using any of the other two 2D estimators; in particular the task is much easier when using the attribute based on the outer product (values of IOQ always below 0.7). Furthermore, image quality indices for these last 2D attributes indicate that distinction between organics, whatever their nature, can be achieved. Such a circumstance enables to progress from a discrete classification according to the hazardous nature towards an accurate identity assignment. This property is highly beneficial in the fight against the threats.

In the case of inorganic salts, any of the 2D attributes is valid to identify sodium chlorate and potassium chlorate, thereby allowing the categorization of a manufactured explosive. As listed in Table 4, even the largest IOQ value of 0.5826 significantly departs from the 0.8 limiting value established for discrimination purposes. However, only the 2D estimator built through the outer product-based approach allows differentiating between cationically-related chlorates and chlorides (IOQ values close to 0).

Summarizing, while the outer-product 2D image elucidates the vast majority of targets, the efficient performance of the other 2D estimators invites to consider the fusion of such attributes as a possible way forward to achieve further synergies. In other words, intermesh the 2D images looking for creating of an almost exclusive identifying pattern for each target. The final purpose is to build a library of identity patterns, thereby enabling to collate, through linear correlation, the unknown interrogated target against those stored.

Table 3
Values for the correlation coefficient (r) and the root mean square error (*RMSE*) estimated between 2D images (used as characteristic fingerprint) of assayed compounds and generated from the outer sum (top) and from the outer product (bottom) of their corresponding normalized Raman and LIBS responses[a].

		Organic materials								Inorganic materials			
		DNT	TNT	RDX	PETN	nylon	wood	riblene	anth	NaCl	$NaClO_3$	KCl	$KClO_3$
Organic materials	DNT		0.1193	0.1907	0.2389	0.3353	0.1547	0.2970	0.1699	0.2544	0.2584	0.1943	0.2161
	TNT	0.7770		0.1705	0.2087	0.3395	0.1939	0.3155	0.2187	0.2497	0.2500	0.1892	0.2097
	RDX	0.3763	0.3526		0.1774	0.3565	0.1786	0.3098	0.2120	0.2458	0.2430	0.1756	0.1932
	PETN	0.1295	0.1565	0.3853		0.3297	0.1953	0.2870	0.2265	0.2703	0.2733	0.2058	0.2149
	nylon	0.6727	0.5172	0.3378	0.2666		0.3533	0.1496	0.2902	0.4645	0.4715	0.3739	0.3661
	wood	0.6493	0.3407	0.4307	0.4488	0.6178		0.2983	0.1483	0.2250	0.2265	0.1740	0.1859
	riblene	0.6346	0.3098	0.3489	0.2639	0.7957	0.7058		0.2322	0.4131	0.4214	0.3196	0.3131
	anth	0.6628	0.2706	0.3015	0.1934	0.6341	0.7758	0.7356		0.2642	0.2738	0.1931	0.2037
Inorganic materials	NaCl	0.1090	-0.0038	0.0038	0.0899	0.1277	0.2580	0.1892	0.3150		0.0779	0.1999	0.2217
	$NaClO_3$	0.0632	-0.0239	0.0169	0.0666	0.1042	0.2382	0.1471	0.2505	0.8870		0.2019	0.2041
	KCl	0.2743	0.0775	0.1740	0.0839	0.2931	0.3857	0.3829	0.4411	0.2362	0.1977		0.0819
	$KClO_3$	0.2043	0.0430	0.1575	0.0883	0.2406	0.3916	0.3195	0.3693	0.2539	0.4102	0.8549	

		Organic materials								Inorganic materials			
		DNT	TNT	RDX	PETN	nylon	wood	riblene	anth	NaCl	$NaClO_3$	KCl	$KClO_3$
Organic materials	DNT		0.0187	0.0294	0.0356	0.0718	0.0278	0.0622	0.0304	0.0278	0.0299	0.0278	0.0323
	TNT	0.6969		0.0249	0.0321	0.0744	0.0235	0.0654	0.0292	0.0235	0.0259	0.0235	0.0285
	RDX	0.1791	0.2861		0.0285	0.0779	0.0235	0.0655	0.0290	0.0235	0.0255	0.0235	0.0276
	PETN	0.0757	0.1624	0.2803		0.0760	0.0320	0.0632	0.0337	0.0320	0.0331	0.0320	0.0345
	nylon	0.5653	0.5219	0.2652	0.2213		0.0868	0.0362	0.0756	0.0868	0.0864	0.0868	0.0858
	wood	NaN	NaN	NaN	NaN	NaN		0.0743	0.0265	0.0000	0.0120	0.0000	0.0181
	riblene	0.4703	0.3602	0.2560	0.2311	0.8586	NaN		0.0628	0.0743	0.0740	0.0743	0.0733
	anth	0.2271	0.1583	0.1060	0.0853	0.3739	NaN	0.3972		0.0265	0.0282	0.0265	0.0303
Inorganic materials	NaCl	NaN	NaN	NaN	NaN	NaN	NaN	NaN	NaN		0.0120	0.0000	0.0181
	$NaClO_3$	-0.0200	-0.0124	0.0131	0.0181	0.0280	NaN	0.0292	0.0195	NaN		0.0120	0.0156
	KCl	NaN	NaN	NaN	NaN	NaN	NaN	NaN	NaN	NaN	NaN		0.0181
	$KClO_3$	-0.0323	-0.0104	0.0324	0.0167	0.0390	NaN	0.0471	0.0201	NaN	0.5161	NaN	

[a] Light-gray cells contain *RMSE* values whereas non colored cells list r values. *NaN* (no available number) reflects the impossibility for computing the parameter when the signal is a matrix completely composed by zeros.

Table 4
Comparison of the universal image index of quality (IOQ) from the second-order attributes generated for several compounds[a].

		Organic compounds								Inorganic compounds			
		DNT	TNT	RDX	PETN	nylon	wood	riblene	anth	NaCl	$NaClO_3$	KCl	$KClO_3$
Organic compounds	DNT		0.8365	0.6453	0.6105	0.3778	0.0018	0.3641	0.6508	0.0018	0.2079	0.0018	0.3936
	TNT	0.8928		0.6752	0.6488	0.4012	0.0012	0.3849	0.6300	0.0012	0.2072	0.0012	0.4024
	RDX	0.8441	0.8493		0.6683	0.4773	0.0012	0.4740	0.6848	0.0012	0.1759	0.0012	0.3718
	PETN	0.7956	0.8595	0.8719		0.6370	0.0030	0.6189	0.6502	0.0030	0.1136	0.0030	0.2532
	nylon	0.6428	0.7180	0.6875	0.7836		0.0012	0.8767	0.4694	0.0012	0.0630	0.0012	0.1466
	wood	0.8216	0.7361	0.7756	0.7420	0.5829		0.0018	0.0012	1.0000	0.0012	1.0000	0.0012
	riblene	0.6650	0.7276	0.7329	0.8132	0.9394	0.6042		0.4526	0.0018	0.0515	0.0018	0.1275
	anth	0.8446	0.8066	0.8491	0.8480	0.7538	0.8093	0.7985		0.0012	0.1680	0.0012	0.3729
Inorganic compounds	NaCl	0.5620	0.5215	0.5127	0.4680	0.3400	0.6409	0.3443	0.4858		0.0012	1.0000	0.0012
	$NaClO_3$	0.5669	0.5301	0.5256	0.4659	0.3329	0.6501	0.3359	0.4928	0.9291		0.0012	0.4915
	KCl	0.8108	0.7921	0.8149	0.7820	0.6423	0.8081	0.6728	0.8330	0.5815	0.5843		0.0012
	$KClO_3$	0.8046	0.7864	0.8187	0.7913	0.6660	0.8121	0.6968	0.8486	0.5527	0.5826	0.9638	

	Organic compounds							Inorganic compounds			
	TNT	RDX	PETN	nylon	wood	riblene	anth	NaCl	$NaClO_3$	KCl	$KClO_3$
DNT	0.6906	0.7511	0.6786	0.2895	0.7579	0.3336	0.6874	0.4607	0.3835	0.6353	0.6353
TNT	0.7134	0.8033	0.4450	0.6132	0.5091	0.6759	0.3648	0.3077	0.6776	0.6634	
RDX	0.7716	0.3919	0.7333	0.4350	0.7256	0.4085	0.3309	0.6576	0.6598		
PETN	0.4908	0.7207	0.5676	0.7818	0.3267	0.2533	0.7364	0.7360			
nylon	0.3943	0.8341	0.5187	0.1344	0.0930	0.4779	0.4817				
wood	0.4468	0.7836	0.3932	0.3177	0.6967	0.7106					
riblene	0.5900	0.1612	0.1139	0.5503	0.5497						
anth	0.3006	0.2267	0.7582	0.7614							
NaCl	0.8747	0.3437	0.3408								
$NaClO_3$	0.2728	0.2671									
KCl	0.9819										
$KClO_3$											

[a] Light-gray cells contain index of quality for 2D images created from the outer product; non-colored cells list the index of quality for outer sum based 2D images and light-blue cells include index of quality for the previous 2D estimators.[10]

3.5. Building and using the identity library

As a final issue, in order to progress the selectivity towards specificity, the combined use of the three bidimensional attributes of each compound (the beforehand [16] and the new ones developed) has been considered for its identifying. The purpose is to build a stock of identities from the assembling of 2D images, thereby allowing that the interrogated target meets its match. Each compound will have a unique identifier, called "*quick identification code*" *(QI-code)*, which will specify the compound completely. In other words, no two compounds may have the same *QI-code*. Drawing on the identical size of all the 2D estimators concerned, their most straightforward combination has been performed. An assembling by concatenation of the images has been considered for generating the *QI-code* of each compound. In doing so, different *QI-codes* were constructed, namely three fused arrays (3330×1665 variables) from the paired combination of the 2D images, and one fused array (4995×1665 variables) when all the 2D attributes are assembled together. Thus, a total of 4 possible storage libraries composed by their particular group of *QI-codes* were built.

The results from libraries' performance evaluation (*data not shown*) contributed to decide the most efficient combination to create the *QI-codes* for the final library: the assembling of the 2D image from the outer product and that from the previous fusion approach [16]. The assembling of images in *landscape* direction proved equivalent to the merging in *portrait* manner.

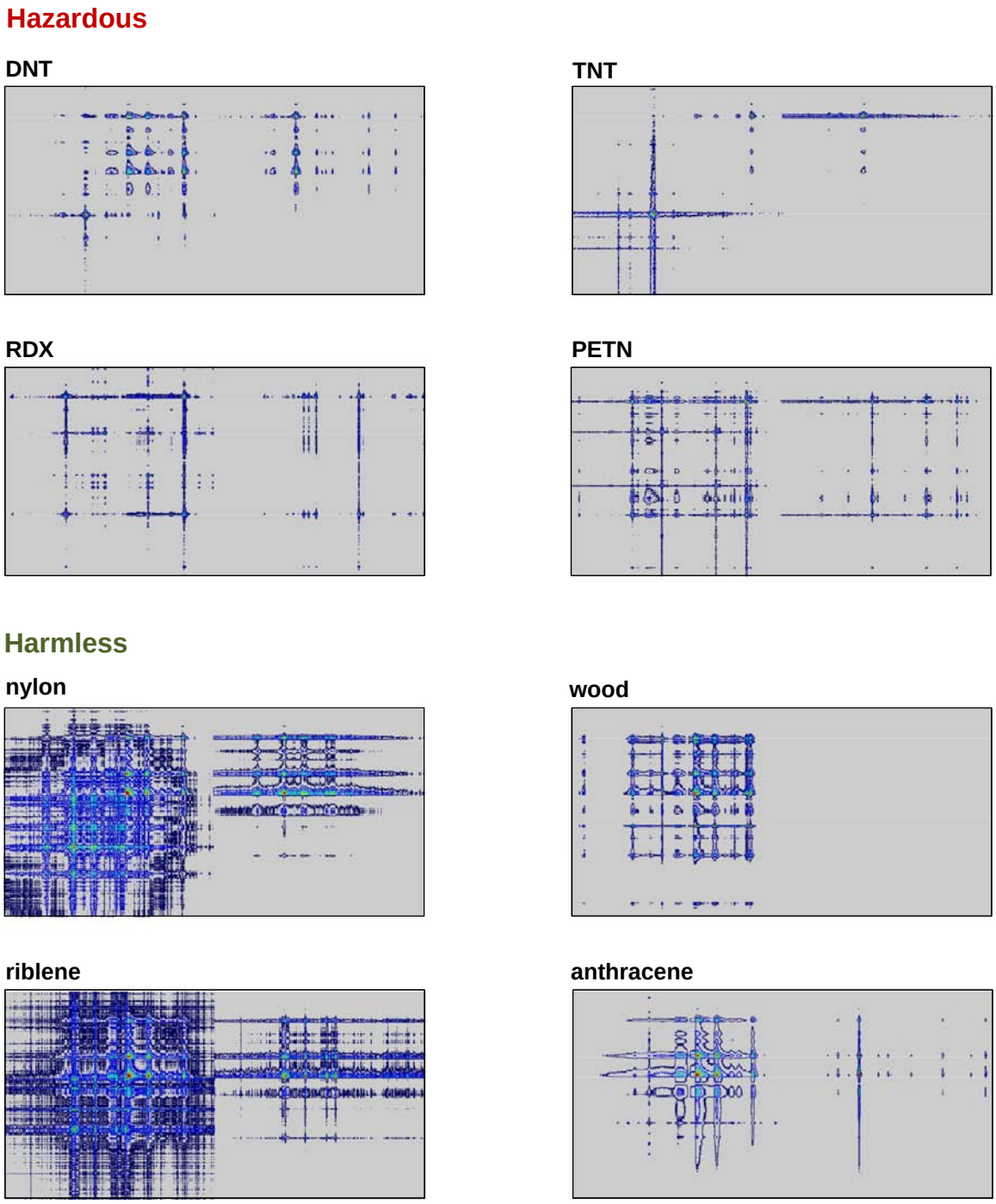

Fig. 4. Examples of the *QI-codes* of some hazardous—DNT, TNT, RDX, PETN—(top) and harmless—nylon, wood, riblene and anthracene—(bottom) organics.

Table 5
Results on search identification of different organics on the basis of the similarity rate (expressed as a correlation coefficient) when the library built with *QI-codes* is implemented to assign the identity.

	DNT	***TNT***	***RDX***	***PETN***	***nylon***	***wood***	***riblene***	***anthracene***
DNT		0.5581 (3)	0.4038 (6)	0.2369 (7)	0.5093 (5)	0.5713 (2)	0.5404 (4)	0.6323 (1)
TNT	0.5581 (1)		0.2582 (5)	0.2778 (4)	0.5024 (2)	0.2369 (6)	0.3061 (3)	0.2179 (7)
RDX	0.4038 (3)	0.2582 (7)		0.3908 (5)	0.3324 (6)	0.4874 (1)	0.3912 (4)	0.4212 (2)
PETN	0.2369 (7)	0.2778 (6)	0.3908 (2)		0.3761 (3)	0.5317 (1)	0.3709 (4)	0.3365 (5)
nylon	0.5093 (4)	0.5024 (5)	0.3324 (7)	0.3761 (6)		0.5118 (3)	0.7942 (1)	0.6084 (2)
wood	0.5713 (3)	0.2369 (7)	0.4874 (6)	0.5317 (4)	0.5118 (5)		0.6078 (2)	0.7859 (1)
riblene	0.5404 (4)	0.3061 (7)	0.3912 (5)	0.3709 (6)	0.7942 (1)	0.6078 (3)		0.6839 (2)
anthracene	0.6323 (3)	0.2179 (7)	0.4212 (5)	0.3365 (6)	0.6084 (4)	0.7859 (1)	0.6839 (2)	

The numbering in brackets arranges the resemblance, in order of decreasing, between the interrogated target and those stored within the library.

Proof on the effectiveness of the final library to identify each compound is shown in Fig. 4, where the *QI-codes* for the considered organics are depicted. Each code is composed by something more than 5 and a half million variables. As seen, differences within the identifiers of *hazardous* compounds and those of *harmless* materials are detectable even to the naked eye. Beyond such *inter-class* differences, the approach even goes as far as to perform an *intra-class* categorization. Table 5 lists the results on the implementation of the library to assign the identity of concerned organics from their *QI-codes*. Data correspond to the similarity rate (expressed as a correlation coefficient) evaluated from a *cross-validation*; that is, when left out from the library the object being checked. As seen, the *QI-code* increases the accuracy on declaring the identity of the interrogated compound. The rates of coincidence between compounds, computed on the basis of this new estimator, decrease as compared to those reached when using any single 2D image as identifier. In no case the frontier of a 0.8 of similarity is exceeded, despite that the identity of the interrogated compound is unavailable in the library. Hence, the most outstanding advantage of this *QI-code* is the capability not only to predict a potential risk, also the competence in assigning the identity of the threat. The approach presented here demonstrates the synergistic effect of LIBS and Raman spectral data when combined in an advanced sensor fusion strategy.

4. Conclusions

In the present manuscript, the pros and cons offered by the different combinations of Raman and LIBS responses of a target to its identification have been drawn. Despite that some materials can be categorized either from their particular molecular or atomic spectral features, the enhancement revealed by an advanced combination of Raman and LIBS has been disclosed. As demonstrated, when the LIBS response is not sufficient for distinction between organics, the fusion with the Raman counterpart leads to substantive improvement in the differentiation ability. Similarly, when Raman spectroscopy cannot report exclusive information on the identity of compounds, progress in categorization from the input of LIBS data is beyond any doubt. In this context, the assembling of the spectral information into bi-dimensional estimators emphasizes more the differences between compounds as compared to their corresponding mono-dimensional attributes. Furthermore, it has been proved that by using a specific code integrated by two 2D estimators, the declaration on the identity of the interrogated target offers an absolute reliability.

The inspected targets are easily identified from the matching of their codes with those previously stored in a small library exhibiting correlation rates far below of 0.8. The proposed data fusion strategy fully exploits the orthogonal atomic and molecular spectral information; thereby proving the synergy of the two spectral counterparts. Further investigation on the robustness and ruggedness of the codes in the identification of compounds in presence of possible interferences as well as complex mixtures, are right now under development. Furthermore, testing on the performance of approaches to identify residues left on surfaces of supports is also in progress.

Acknowledgements

This work was supported by Project CTQ11-24433 of the Ministerio de Economía y Competitividad, Secretaría de Estado de Investigación, Desarrollo e Innovación of Spain and from the Consejería de Innovación, Ciencia y Empresa de la Junta de Andalucía (Project P07-FQM-03308).

References

[1] L. Hall, J. Llinas, Proc. IEEE 85 (1997) 6–23.
[2] N. Salim, J. Holliday, P. Willett, J. Chem. Inf. Comput. Sci. 43 (2003) 435–442.
[3] G.W. Geerling, M. Labrador-Garcia, J.G.P.W. Clevers, A.M.J. Ragas, A.J.M. Smits, Int. J. Remote Sens 28 (2007) 4263–4284.
[4] J. Forshed, H. Idborg, S.P. Jacobsson, Chemom. Intell. Lab. Syst 85 (2007) 102–109.
[5] A. Smolinska, L. Blanchet, L. Coulier, K.A.M. Ampt, T. Luider, R.Q. Hintzen, S.S. Wijmenga, L.M.C. Buydens, PLoS One 7 (2012) e38163.
[6] C.V. Di Anibal, M.P. Callao, I. Ruisánchez, Talanta 84 (2011) 829–833.
[7] Y.B. Monakhova, R. Godelmann, A. Hermann, T. Kuballa, C. Cannet, H. Schafer, M. Spraul, D.N. Rutledge, Anal. Chim. Acta 833 (2014) 29–39.
[8] S. Mas, R. Tauler, A. de Juan, J. Chromatogr. A 1218 (2011) 9260–9268.
[9] F.C. Clarke, M.J. Jamieson, D.A. Clark, S.V. Hammond, R.D. Jee, A.C. Moffat, Anal. Chem. 73 (2001) 2213–2220.
[10] P.M. Ramos, I. Ruisánchez, K.S. Andrikopoulos, Talanta 75 (2008) 926–936.
[11] T.I. Dearing, W.J. Thompson, C.E. Rechsteiner, B.J. Marquardt, Appl. Spectrosc. 65 (2010) 181–186.
[12] M. Casale, N. Sinelli, P. Oliveri, V. Di Egidio, S. Lanteri, Talanta 80 (2010) 1832–1837.
[13] S.J. Tao, J.M. Li, J.H. Li, J.B. Tang, J.R. Mi, L.L. Zhao, IFIP Adv. Inf. Commun. Technol. 369 (2012) 478–483.
[14] L. Vera, L. Acena, J. Guasch, R. Boque, M. Mestres, O. Busto, Talanta 87 (2011) 136–142.
[15] H.W. Lee, A. Christie, J. Xu, S. Yoon, Biotechnol. Bioeng. 109 (2012) 2819–2828.
[16] J. Moros, J.J. Laserna, Anal. Chem. 83 (2011) 6275–6285.
[17] J.S. Caygill, F. Davis, S.P.J. Higson, Talanta 88 (2012) 14–29.
[18] F.J. Fortes, J.J. Laserna, Spectrochim. Acta, Part B 65 (2010) 975–990.
[19] D.S. Moore, R.J. Scharff, Anal. Bioanal. Chem. 393 (2009) 1571–1578.
[20] J. Moros, F.J. Fortes, J.M. Vadillo, J.J. Laserna, LIBS detection of explosives in traces, in: S. Musazzi, U. Perini (Eds.), Laser-Induced Breakdown Spectroscopy, Springer-Verlag, Berlin, 2014, pp. 349–375.
[21] J. Moros, J.A. Lorenzo, K. Novotný, J.J. Laserna, J. Raman Spectrosc. 44 (2013) 121–130.
[22] J. Moros, J.A. Lorenzo, P. Lucena, L.M. Tobaria, J.J. Laserna, Anal. Chem. 82 (2010) 1389–1400.
[23] J. Moros, J.A. Lorenzo, J.J. Laserna, Anal. Bioanal. Chem. 400 (2011) 3353–3365.
[24] P.V. Shah, A. Singh, S. Agarwal, S. Sedigh, A. Ford, R. Waterbury, Proc. SPIE 7303 (2009) 730329.
[25] Z. Wang, A.C. Bovik, IEEE Signal Proc. Let 9 (2002) 81–84.